Electronic Supplementary Information

Molten Multi-Phase Catalytic System Comprising Li-Zn Alloy and LiCl-KCl Salt for Nitrogen Fixation and Ammonia Synthesis at Ambient Pressure

Xian Meng[1,#], Jian Liu[1,#], Zujian Tang[1], Bingxu Xi[1], Pu Yan[1], Xiangran Wang[1], Kecheng Cao[1], Bo Yang[1,**], Xiaofei Guan[1,*]

[1] School of Physical Science and Technology, ShanghaiTech University, 393 Huaxia Middle Road, Shanghai, 201210, China

[#] These authors contributed equally

[*] E-mail: guanxf@shanghaitech.edu.cn (X.G.)

[**] E-mail: yangbo1@shanghaitech.edu.cn (B.Y.)

Contents:

Table S1. Chemicals used in all experiments.

Chemical	Brand	Purity
Li	Sinopharm	>99.9%
Zn	Sinopharm	≥99.8%
KCl	Sinopharm	≥99.8%
LiCl	Titan	≥99%
NH4Cl	Titan	>99.9%
HOC_6H_4COONa	Titan	>99.5%
LiH	Macklin	>97%
NaOH	Macklin	>98%
$LiNH_2$	J&K	95%
$C_4H_4KNaO_6$ $4H_2O$	J&K	99%
$C_5FeN_6Na_2O$ $2H_2O$	Aladdin	99.98%
H_2SO_4	Sinopharm	98%, analytical reagent
HCl	Sinopharm	36.5%, CP
NaClO*****	Sinopharm	chemically pure
$NiCl_2$	Macklin	99%
H_2O	Macklin	deionized
N_2	Youjiali Special Gas Co., Ltd	99.999%
H_2	Youjiali Special Gas Co., Ltd	99.999%
Ar	Youjiali Special Gas Co., Ltd	99.999%

***** Cl concentration > 5.2%, free alkali concentration: 7~8%.

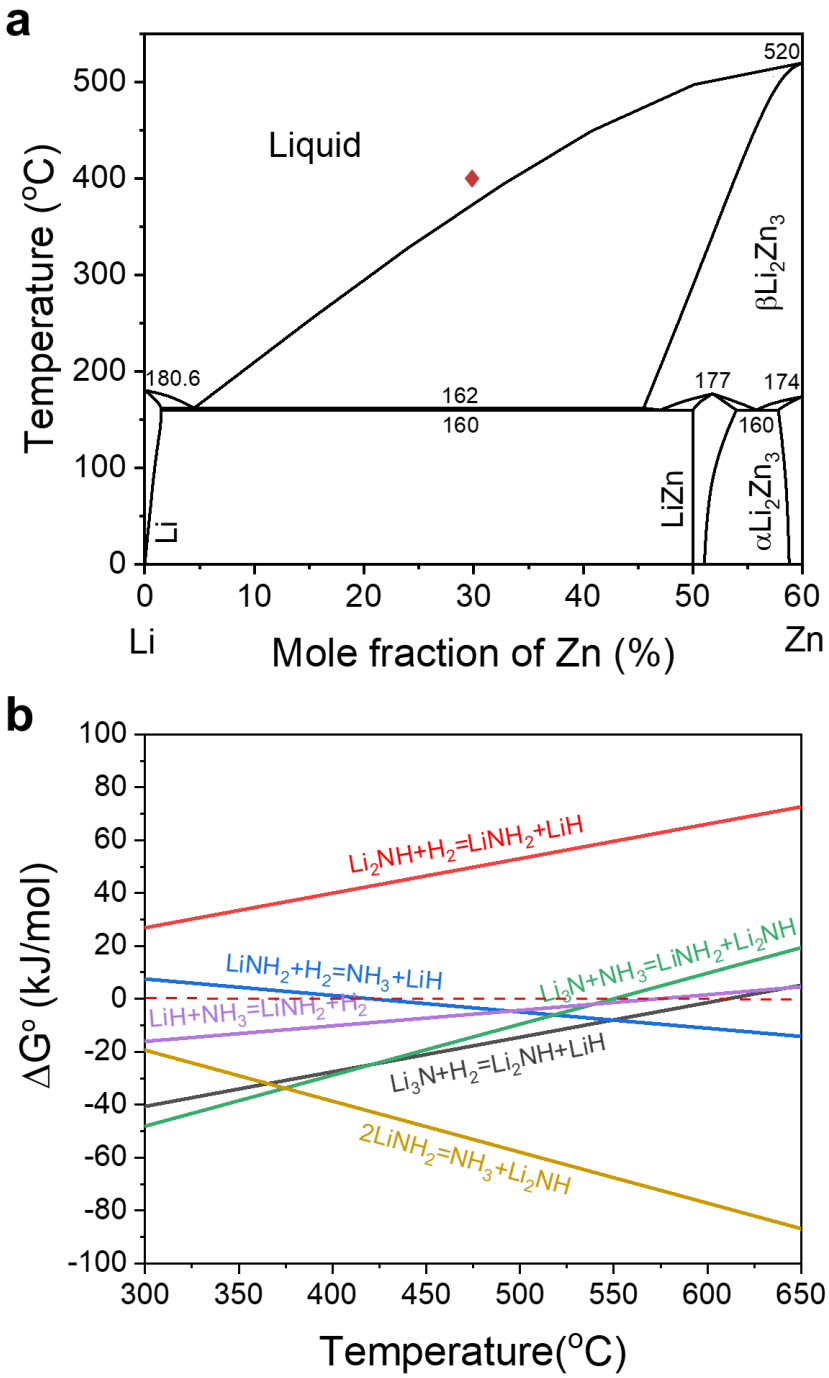

Figure S1. (a) The Li-Zn phase diagram modified after Okamoto[1]. (b) Standard Gibbs free energy change (ΔG^o) for reactions in the Li-N-H system[2-4]. The red dashed line was a horizontal line passing through the zero point of the Y axis.

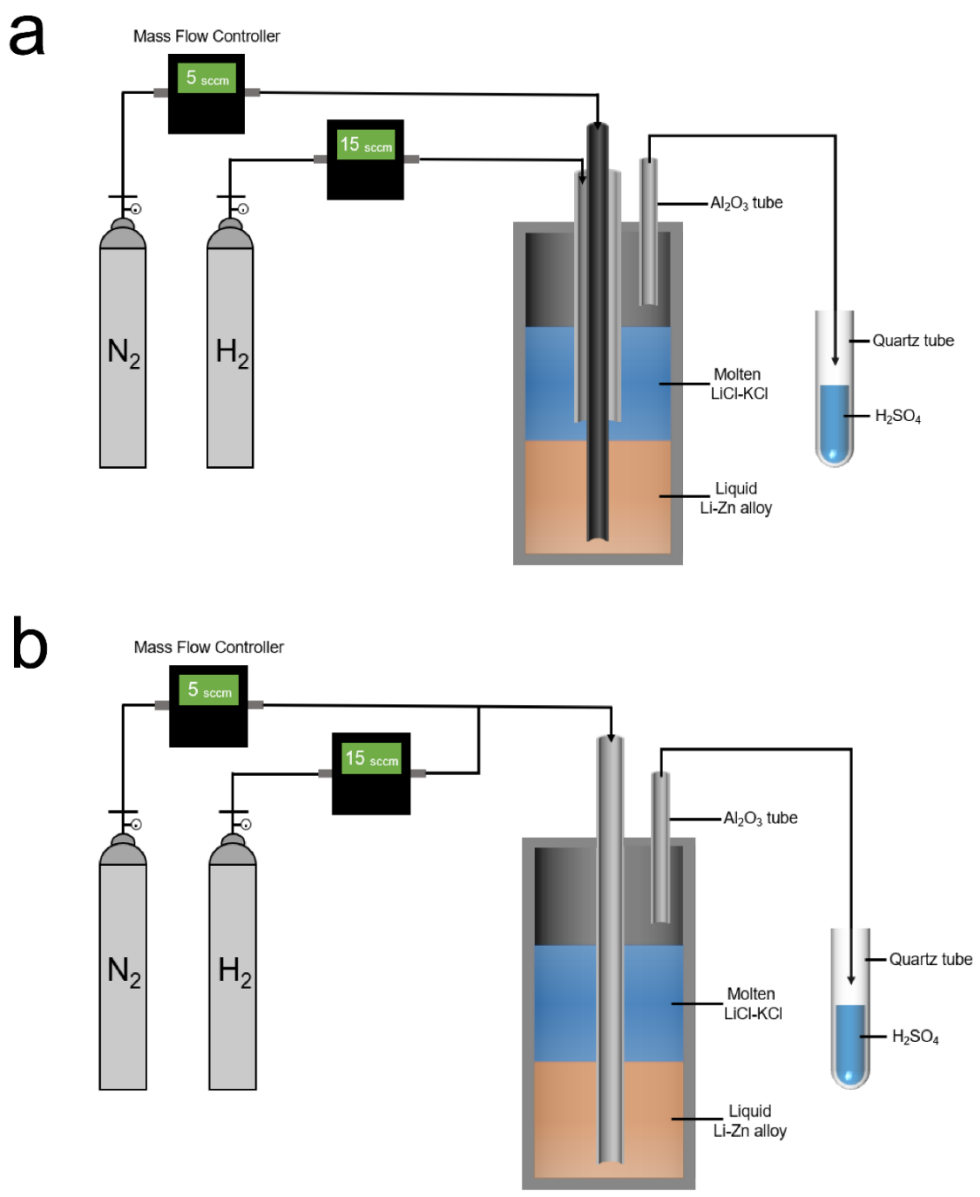

Figure S2. Schematic diagrams of the bubble column reactors for NH_3 synthesis. (a) N_2 was introduced into the bottom of the liquid alloy through an alumina bubbling tube (OD: 3 mm; ID: 1 mm; length: 650 mm). H_2 was introduced into the bottom of the molten salt through an alumina bubbling tube (OD: 6 mm; ID: 4 mm; length: 500 mm). The two bubbling tubes were coaxial. (b) A mixture of N_2 and H_2 was introduce into the bottom of liquid alloy through an alumina bubbling tube (OD: 6 mm; ID: 4 mm; length: 600 mm). The external gas pipelines used were made of Teflon fluoropolymers.

Table S2. The starting amounts of materials (including metals and salts) used for the ammonia synthesis experiments. The superscripts *a* and *b* in the table represent the amount of metals required for different experimental setups as illustrated in Figures S2 (a) and (b), respectively. The target height of the Li-Zn liquid alloy was 5 cm. The target height of the molten eutectic LiCl-KCl was 5, 10 or 15 cm.

Systems	Temperature (ºC)	Li-Zn alloy		LiCl-KCl salt	
		Li (g)	Zn (g)	LiCl (g)	KCl (g)
70mol%Li-Zn (5 cm) and eutectic LiCl-KCl (5 cm)	400	2.900[a]	11.709[a]	3.978	4.822
		2.532[b]	10.223[b]		
70mol%Li-Zn (5 cm) and eutectic LiCl-KCl (10 cm)	400	2.532[b]	10.223[b]	7.957	9.643
70mol%Li-Zn (5 cm) and eutectic LiCl-KCl (15 cm)	400	2.532[b]	10.223[b]	11.935	14.465
70mol%Li-Zn (5 cm) and eutectic LiCl-KCl (5 cm)	500	2.899[a]	11.704[a]	4.029	4.882

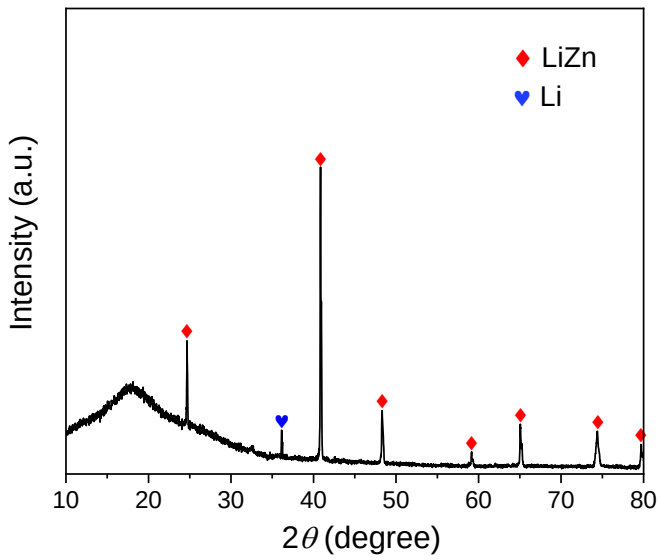

Figure S3. The XRD pattern of the pretreated Li-Zn mixture showing the characteristic peaks for LiZn (PDF No. 03-0954) and Li (PDF No. 01-074-6889).

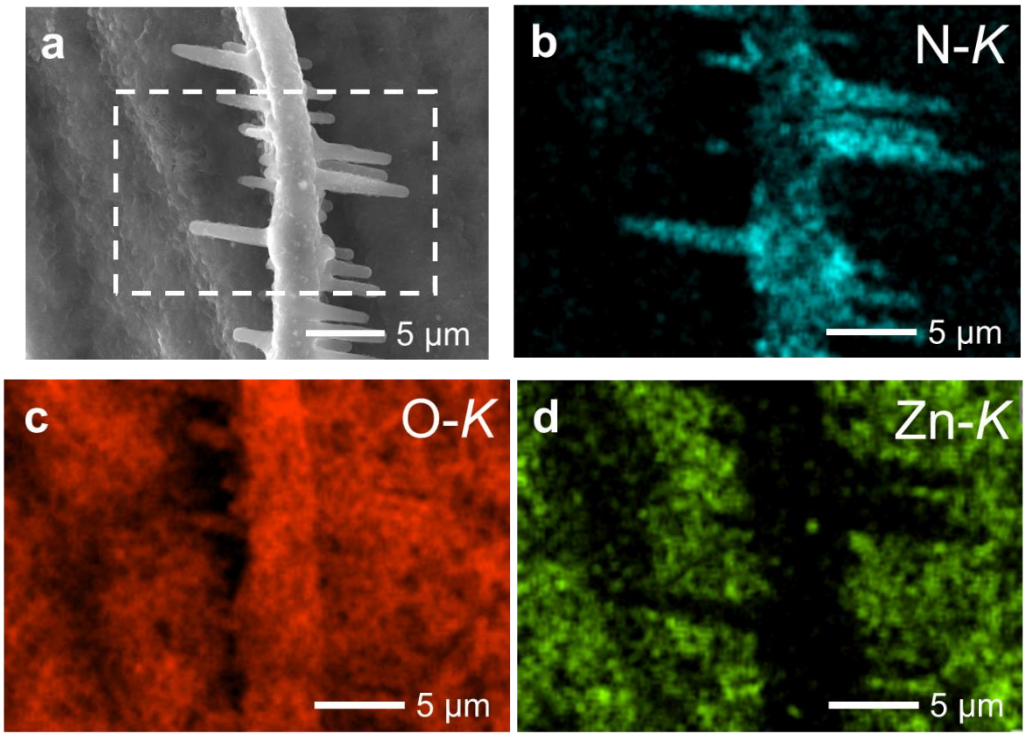

Figure S4. (a) SEM image of the sample 2 collected from the top of the solidified alloy column after the reaction with N_2 in the molten state. (b) N-*K*, (c) O-*K*, and (d) Zn-*K* EDS elemental mapping for the area enclosed by the white dashed rectangle in (a). The presence of the O as shown in (c) was likely due to the Li oxidation or the Li_3N hydrolysis during the SEM sample preparation and transfer outside the Ar-filled glovebox. (b) and (d) show that the distributions of N and Zn were complementary, indicating that no Zn_3N_2 was formed and the Li played the key role of fixing nitrogen in the Li-Zn alloy. The SEM and EDS results suggest that the Li_3N exhibited a dendrite-like shape on top of the Li-Zn alloy as shown in (a).

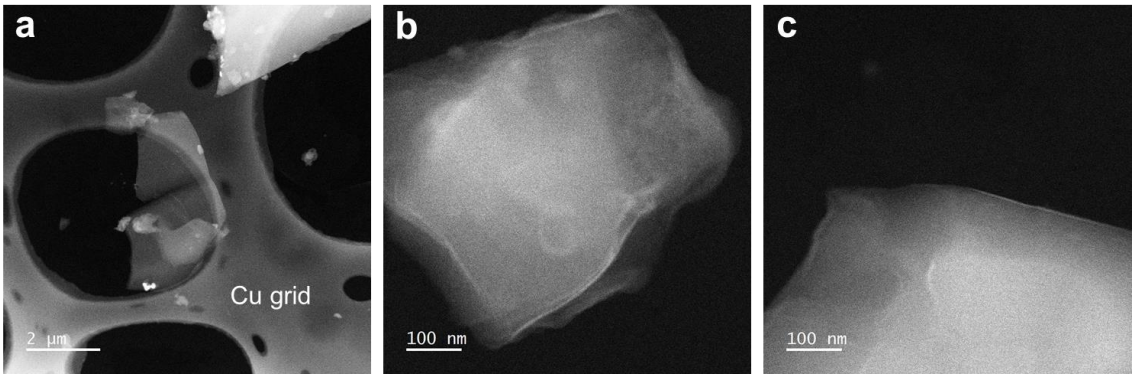

Figure S5. STEM images showing the particles of sample 1 on a copper grid.

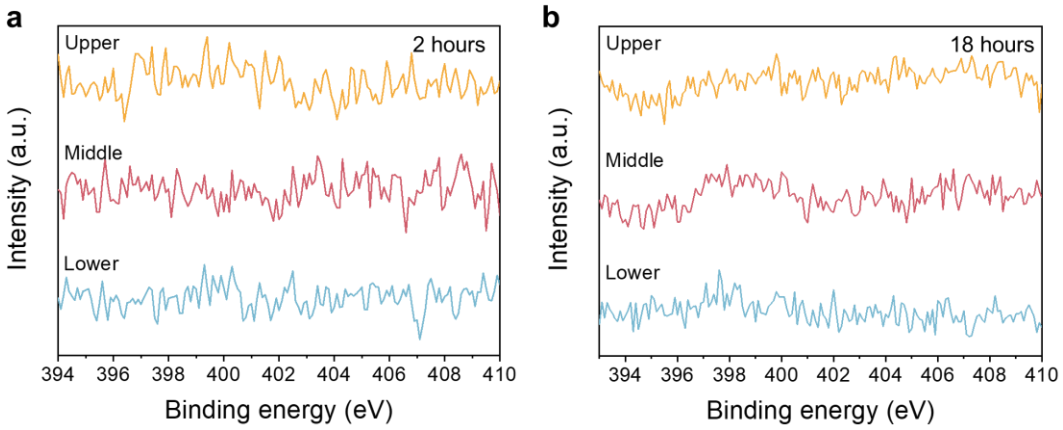

Figure S6. Representative N 1*s* XPS results of the upper, middle, lower parts of the solidified alloy columns after the reaction with N_2 for (a) 2 hours and (b) 18 hours at 400 ℃. No characteristic peaks for N 1*s* were identified, confirming the absence of Li_3N in the alloy.

Table S3. The N weight fraction in the solidified salt in the experiments that operated for different durations at 400 ℃. For each experiment, five salt samples were characterized. The N weight fraction was calculated by subtracting the amount of nitrogen in the impurities in the commercial eutectic LiCl-KCl (0.01847wt.%) and then taking the mass-weighted average.

Reaction duration (h)	Sample No.	Sample mass (g)	N weight fraction after subtracting the N impurities in the salt (wt.%)	N weight fraction in the salt obtained by taking the mass-weighted average (wt.%)
0.5	1	0.1916	0.167	0.163
	2	0.1828	0.163	
	3	0.1862	0.162	
	4	0.2026	0.163	
	5	0.2081	0.161	
1	1	0.1866	0.409	0.394
	2	0.1878	0.376	
	3	0.2105	0.377	
	4	0.1842	0.409	
	5	0.1663	0.402	
2	1	0.1481	0.530	0.555
	2	0.1834	0.557	
	3	0.1930	0.562	
	4	0.1589	0.545	
	5	0.1507	0.582	
3	1	0.1075	1.083	1.025
	2	0.0937	1.001	
	3	0.1130	0.901	
	4	0.1107	1.098	
	5	0.1115	1.043	
4	1	0.1358	1.669	1.218
	2	0.1808	1.222	
	3	0.1394	1.141	
	4	0.1422	0.982	
	5	0.2310	1.140	
10	1	0.0542	1.906	1.934
	2	0.0694	1.897	
	3	0.0694	2.054	
	4	0.0780	2.070	
	5	0.1005	1.785	
18	1	0.0930	2.626	2.655
	2	0.0895	3.500	
	3	0.0691	3.266	
	4	0.0870	2.473	
	5	0.0953	1.611	

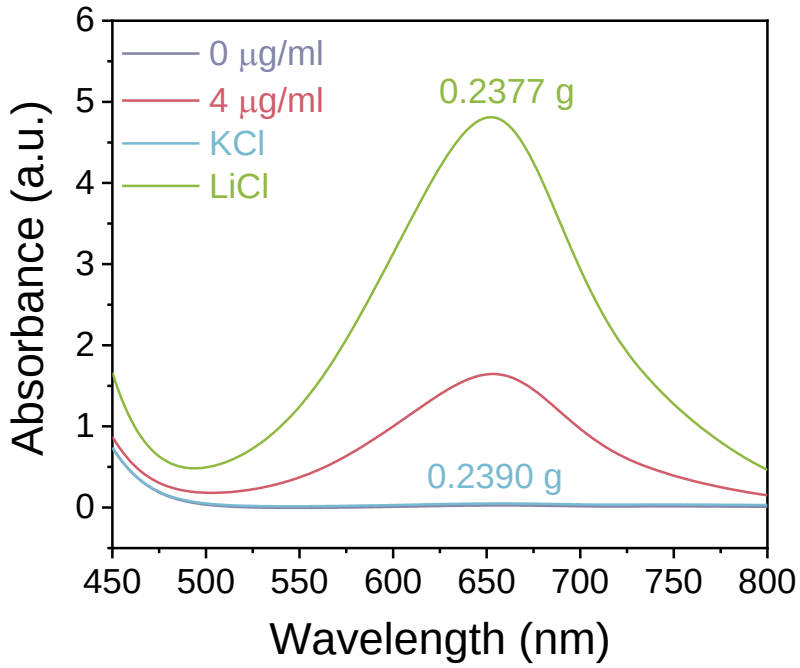

Figure S7. UV-Vis spectra for determining the nitrogen weight fraction in the commercial LiCl and KCl used in the experiments. The sample solutions were prepared by first dissolving LiCl (0.2377 g) and KCl (0.239 g) in 10 ml H_2SO_4 solutions, respectively. The UV-Vis spectra for the standard solutions with 0 and 4 μg(NH_3)/ml are also shown. Based on the results, the nitrogen weight fraction in the commercial eutectic LiCl-KCl was estimated to be 0.0185wt.%.

Note S1. Measurement of the Apparent Activation Energy for N_2 Fixation by the Li-Zn Liquid Alloy

The N_2 fixation rate by the liquid 70mol%Li-Zn alloy was obtained by measuring the amount of the nitrogen dissolved in the molten salt phase at different temperatures (380, 400, 425, and 450 °C) for 2 hours. N_2 was bubbled to the liquid 70mol%Li-Zn alloy at 5 cm^3/min, and Ar was introduced into the molten LiCl-KCl salt at 15 cm^3/min to homogenize the distribution of Li_3N in the molten salt. Before cooling down, Ar bubbling was kept for another 30 mins to ensure the full dissolution and diffusion of Li_3N.

For each experiment, three or five pieces of the solidified salt were sampled randomly, weighed, and then dissolved in 10 ml of 0.05mol/L H_2SO_4 inside an ultrasonic instrument. The liquid solutions were characterized using UV-Vis spectroscopy to determine the nitrogen content. Then, the average value of the nitrogen weight fraction in the salt (*N wt%*) was obtained. The N_2 fixation rate was then calculated using Eq. S1, where $M_{LiCl\text{-}KCl}$ is the total mass of the LiCl-KCl salt (8.8 g) used in each experiment.

$$\text{Fixation rate}_{N_2} = \frac{N\ wt\% \times M_{LiCl-KCl}}{reaction\ time} \quad \text{(S1)}$$

From the N_2 fixation rates measured at different temperatures, the apparent activation energy for N_2 (E_{a,N_2}) was determined by using Eq. S2, where *A* is the reaction rate constant, *R* is the gas constant, *T* is the temperature.

$$\text{Fixation rate}_{N_2} = Aexp\left(-\frac{E_{a,N_2}}{RT}\right) \quad \text{(S2)}$$

By taking a natural log of Eq. S2, the following equation can be obtained

$$\ln(\text{Fixation rate}_{N_2}) = lnA - \frac{E_{a,N_2}}{RT} \quad \text{(S3)}$$

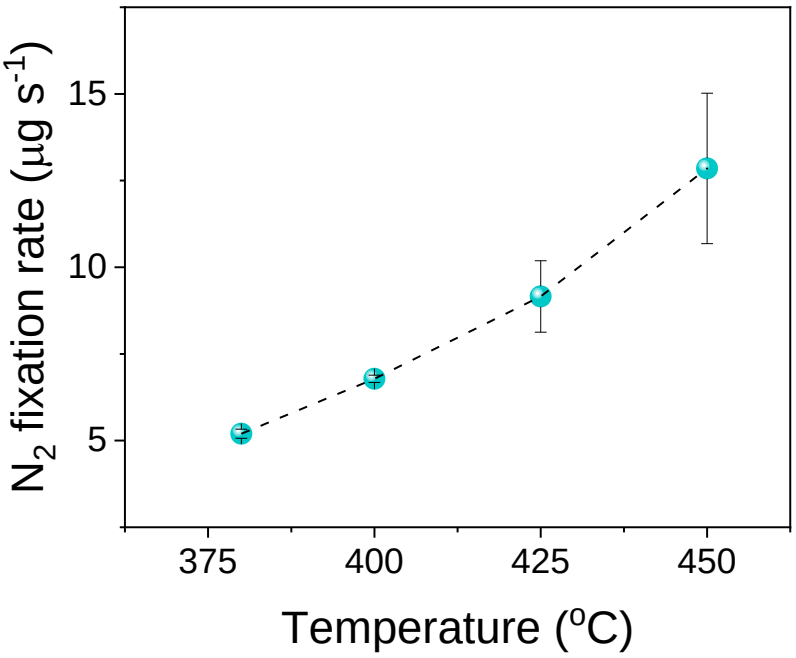

Figure S8. Temperature dependence of the N_2 fixation rate in the reactors containing liquid 70mol%Li-Zn alloy (height: 5 cm) and molten LiCl-KCl salt (height: 5 cm) at different temperatures. The dashed lines serve as the guide for the eyes.

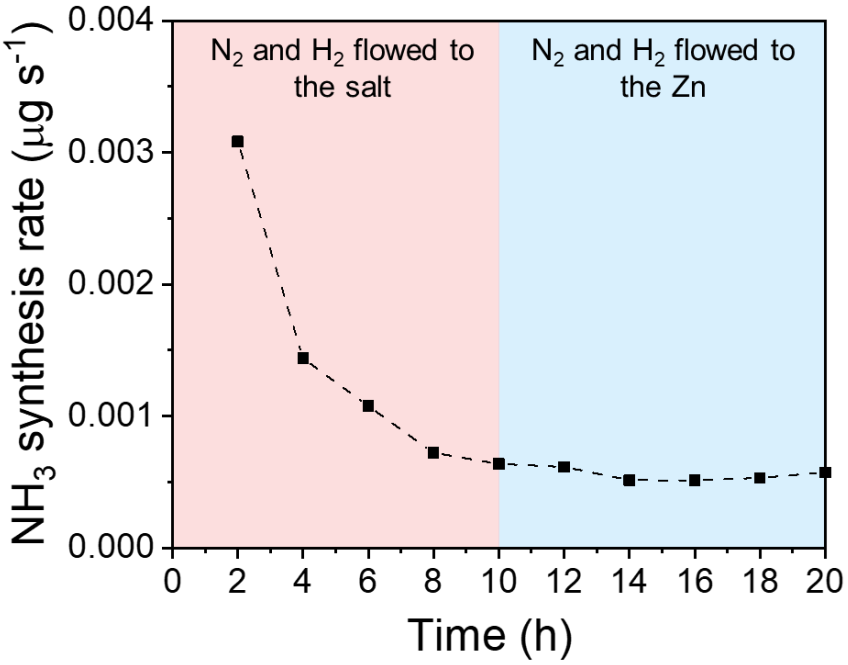

Figure S9. NH_3 synthesis rate in the molten catalytic system comprising the liquid Zn (height: 5 cm) underneath and the LiCl-KCl eutectic salt (height: 5 cm) on the top at 500 ℃. To remove the effect of nitrogen-containing impurities in the molten salt, N_2 (5 cm^3/min) and H_2 (15 cm^3/min) were mixed and then fed into the molten salt in the first 10 hours. The NH_3 synthesis rate decreased from 0.0031 μg/s to 0.0006 μg s^{-1} over 10 hours, indicating the effective removal of the nitrogen-containing impurities. Afterwards, the N_2-H_2 mixture was directly fed into the liquid Zn underneath. No noticeable change in the NH_3 synthesis rate was observed. In other words, the NH_3 synthesis rate remained negligibly small over the following 10 hours.

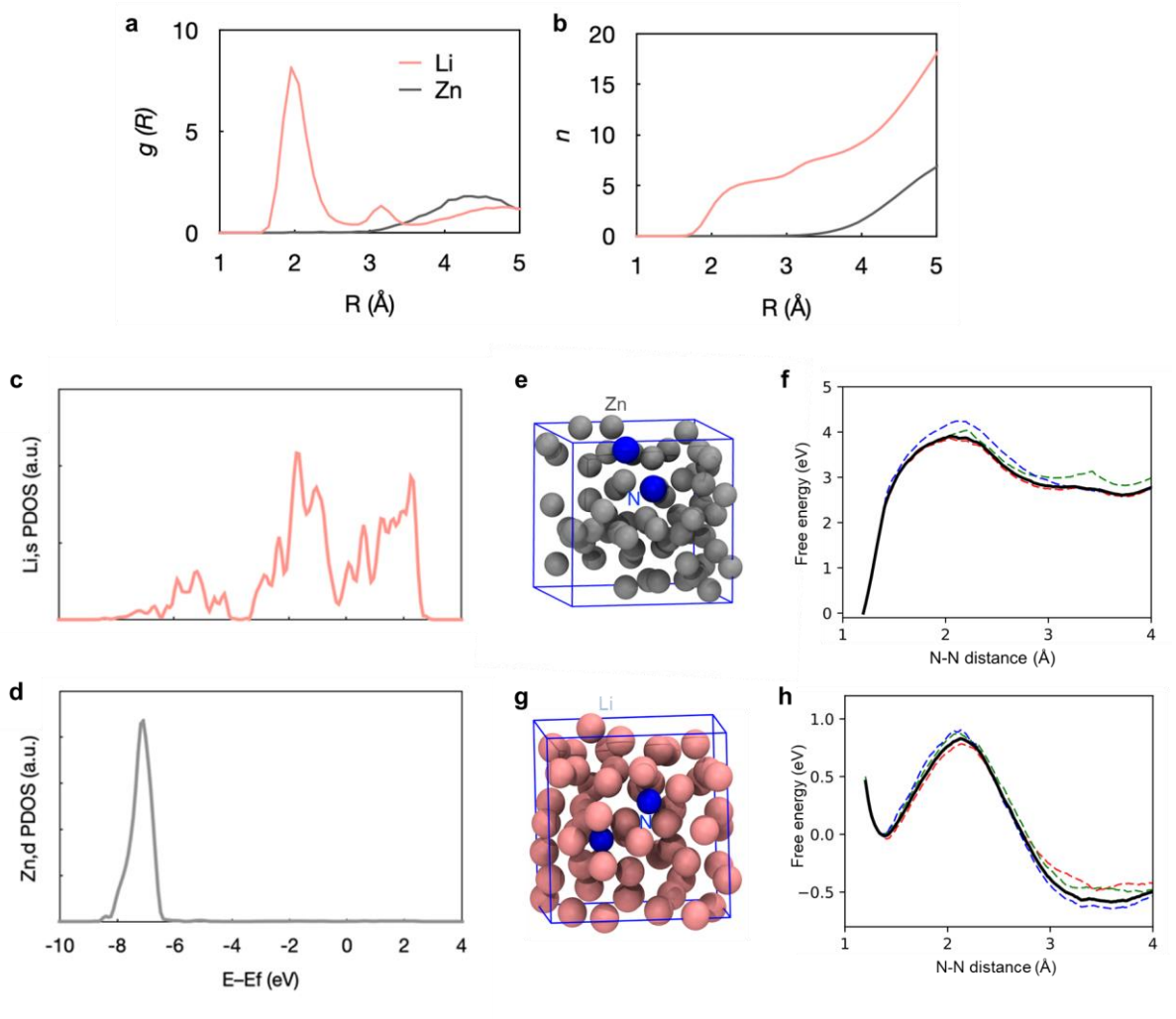

Figure S10. (a) Radial distribution functions, *g(R)*, of Li or Zn atoms and (b) the average number of Li or Zn atoms, *n*, around the N atoms in N_2 obtained from the pre-relax simulation of the Li-Zn system from 3 ps to 5 ps. *R* is the distance from the tagged N atoms. The projected density of states (PDOS) of (c) Li-*s* orbital and (d) Zn-*d* orbital in the Li-Zn model system. (c) and (d) share the same X-axial label.

(e) Snapshot of the bare Zn model system at the end of the AIMD simulation (color code: grey, Zn; blue: N). (f) The free energy change as a function of the N-N distance for the N_2 cleavage in pure liquid Zn at 450 ℃. The work profiles of 3 slow-growth trajectories are also shown, as denoted by the dashed lines in color.

(g) Snapshot of the bare Li model system at the end of the AIMD simulation (color code: pink, Li; blue, N). (h) The free energy profile as a function of the N-N distance for N_2 cleavage in pure liquid Li at 450 ℃.

Note S2. The reactivity of N_2 cleavage in liquid pure Zn and pure Li

A liquid pure Zn (60 atoms) model was built in a periodic cubic cell with the edge length = 11.2 Å, and a N_2 molecule was placed inside. The cubic box represents the periodic unit cell of the infinite bulk system. The AIMD simulations were performed at 450 ºC, slightly greater than the melting point of Zn (419.5 ºC). Figure S10e shows a snapshot of the model system at the end of the simulation. Figure S10f shows the free energy change for the N_2 cleavage to two $N^{\delta-}$ as a function of the N-N distance. The value of δ was calculated to be only 1.4 based on the Bader charge analysis, suggesting the covalent nature of the Zn-N bond. The activation free energy was identified to be as high as nearly 4 eV, and the reaction free energy was almost 3 eV, suggesting that the N_2 cleavage was difficult in pure liquid Zn.

Similarly, a liquid pure Li (60 atoms) model was built and studied with AIMD simulations (Figure S10g,h).

Note S3. The reactivity of N_2 cleavage in liquid Li-Sn

A randomly mixed $Li_{36}Sn_{24}$ model was built in a periodic cubic cell with the edge length = 11.2 Å, and a N_2 molecule was placed inside the cell. The AIMD simulations were performed at 500 ºC. Figure S11a shows a snapshot of the system at the end of the AIMD simulation. Figure S11b shows the free energy change for the N_2 cleavage to two $N^{\delta-}$ as a function of the N-N distance. The value of δ was calculated to be 2.9 based on the Bader charge analysis. The N_2 cleavage in the liquid Li-Sn alloy showed a G_a of 1.7 eV and ΔG of 0.7 eV. A comparison with the results for Li-Zn shows that Li-Zn is more reactive than Li-Sn for activating and fixing N_2.

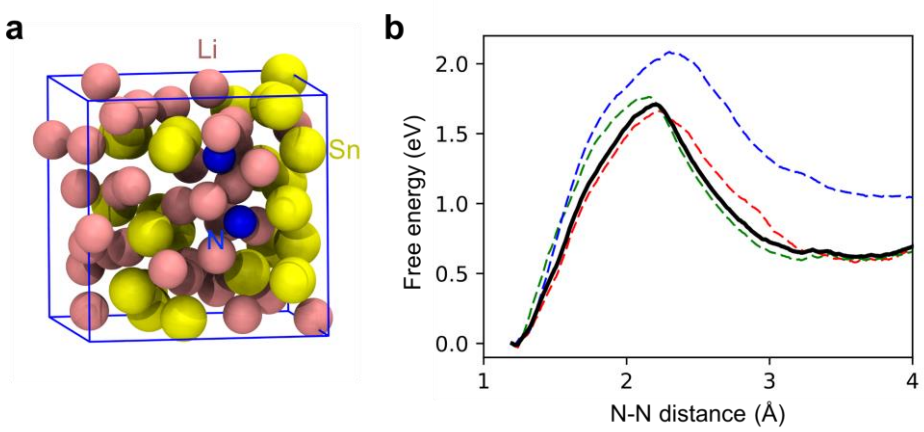

Figure S11. (a) Snapshot of the model system at the end of the AIMD simulation. Color code: pink, Li; yellow, Sn; blue: N. (b) The free energy change as a function of the N-N distance for the N_2 cleavage in 60mol%Li-Sn alloy at 500 ℃. The work profiles of 3 slow-growth trajectories are also shown, as denoted by the dashed lines in color.

Note S4. Synthesis of Li_3N from pure Li and N_2

To synthesize the Li_3N, pure Li tablets were placed in an alumina boat inside an alumina reactor (OD: 35 mm, ID: 28 mm, length: 400 mm), and heated it at 100 ℃ under N_2 flow (20 cm^3/min) for 18 hours. The reactor was sealed by vacuum flanges to prevent oxidation of Li. The phase of the Li_3N synthesized was verified by X-ray diffraction, as shown in Figure S12a. A digital photograph of some pieces of Li_3N is shown in Figure S12b.

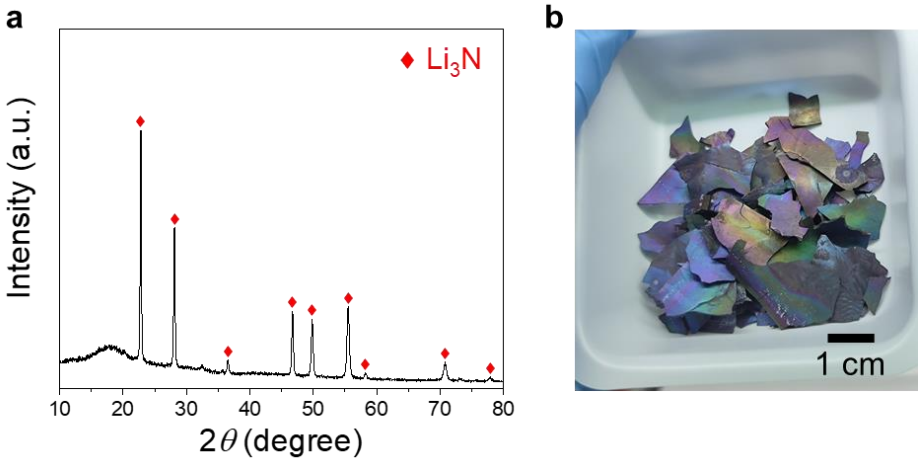

Figure S12. (a) The XRD pattern of the sample after the solid pure Li tablets reacting with N_2. Characteristic peaks for Li_3N (PDF No. 76-0593) were indexed. (b) Digital photo of some Li_3N samples inside a plastic weigh boat.

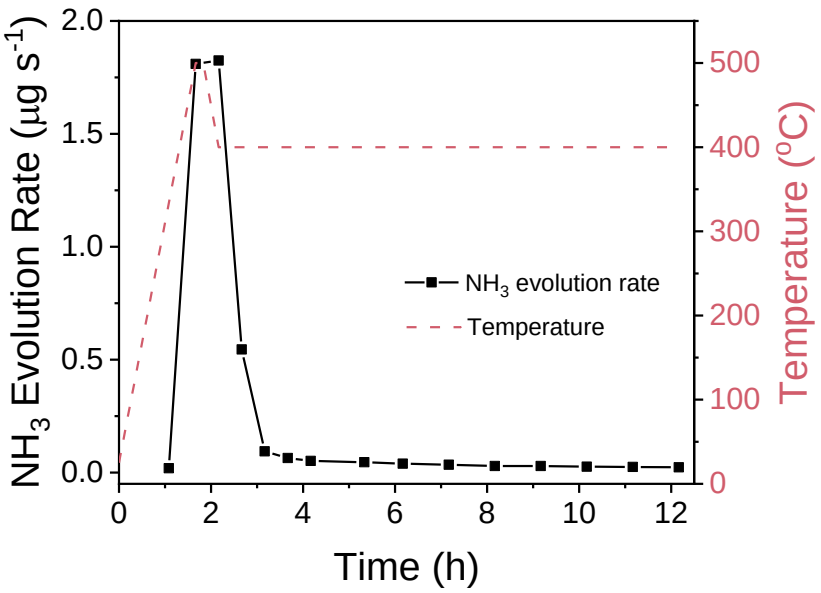

Figure S13. Temperature profile and the rate of NH_3 evolution from the LiCl-KCl-1mol%$LiNH_2$ heated under Ar atmosphere over time. The mass of the eutectic LiCl-KCl was 8.8 g, and the mass of $LiNH_2$ was 0.0368 g. The molten salt height was 5 cm. The ammonia evolution rate first increased and then decreased. Based on the total amount of NH_3 collected, the $LiNH_2$ conversion was calculated to be 69.17%.

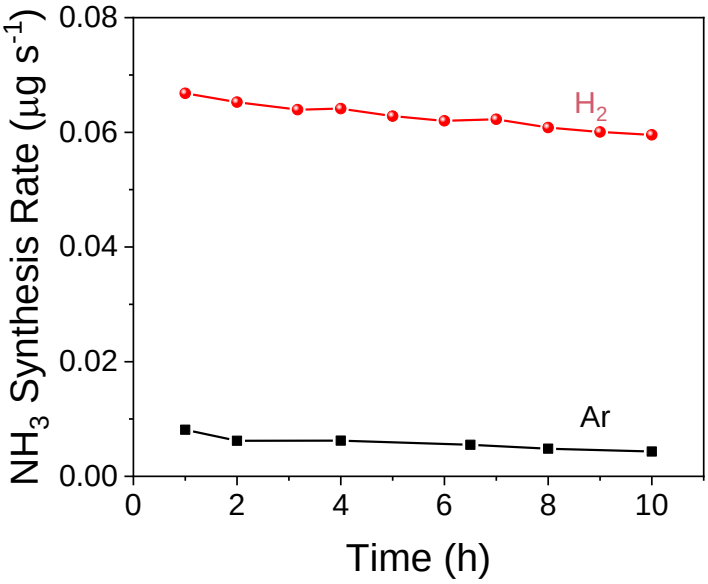

Figure S14. The NH_3 synthesis rate over time in the experiments of bubbling H_2 (15 cm^3/min) or Ar (20 cm^3/min) into molten eutectic LiCl-KCl containing 1mol% Li_2NH at 400 ℃. The height of the molten salt in each experiment was 5 cm. A comparison of the results confirms that the H_2 reacts with the Li_2NH and produces NH_3. As the reaction between H_2 and Li_2NH occurs stepwise via the formation of $LiNH_2$ to produce ammonia, the results also indicate the occurrence of the reaction between H_2 and $LiNH_2$.

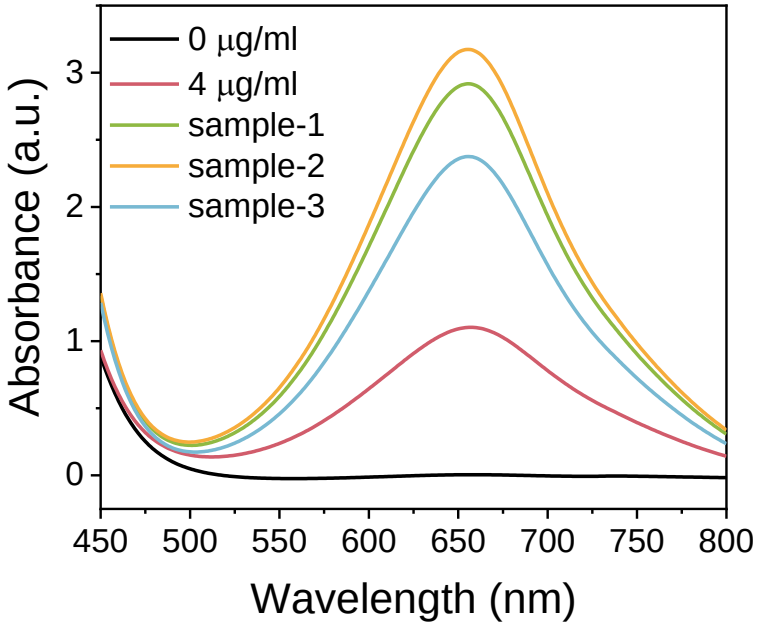

Figure S15. UV-Vis spectra for three solidified salt samples collected randomly from the experiment bubbling N_2 into LiCl-KCl molten salt containing 3mol%LiH at 400 ºC. The masses of the samples 1 to 3 were 0.1718 g, 0.1856 g and 0.1527 g, respectively. The UV-Vis spectra for the standard solutions with 0 and 4 $\mu g_{(NH_3)}$/ml are also shown.

Note S5. Calculation of the degree of nitridation of LiH dissolved in molten LiCl-KCl eutectic salt.

1) NH_3 synthesis: It is assumed that all the H in obtained NH_3 comes from LiH, that is, $3n_{LiH} = n_{NH_3}$.

$$m_{LiH,1} = \frac{3 \times m_{NH_3} \times M_{LiH}}{M_{NH_3}}$$

2) Li_2NH Synthesis: It is assumed that all the N in salt comes from Li_2NH, and N is evenly distributed in salt after the experiment, that is, $n_{Li_2NH} = n_N$.

$$m_{LiH,2} = \frac{2 \times N\ \ wt\% \times m_{salt} \times M_{LiH}}{M_N}$$

Therefore,

$$\text{Degree of nitridation} = \frac{m_{LiH,1} + m_{LiH,2}}{m_{LiH,add}} \times 100\%$$

Table S4. Nitrogen weight fraction in the solidified samples from different experiments.

System	Gas feeding mode	Temperature (°C)	N weight fraction in the solidified salt
70mol%Li-Zn (height: 5 cm) and eutectic LiCl-KCl salt (height: 5 cm)	Separate (N_2 into the alloy; H_2 into the salt)	400	0.559wt.%
70mol%Li-Zn (height: 5 cm) and eutectic LiCl-KCl salt (height: 5 cm)	Separate (N_2 into the alloy; H_2 into the salt)	500	0.783wt.%
70mol%Li-Zn (height: 5 cm) and eutectic LiCl-KCl salt (height: 5 cm)	Mixed (N_2 and H_2 mixture into the alloy)	400	0.407wt.%
70mol%Li-Zn (height: 5 cm) and eutectic LiCl-KCl salt (height: 10 cm)	Mixed (N_2 and H_2 mixture into the alloy)	400	0.304wt.%
70mol%Li-Zn (height: 5 cm) and eutectic LiCl-KCl salt (height: 15 cm)	Mixed (N_2 and H_2 mixture into the alloy)	400	0.276wt.%

Note S6. Validation Experiment on the Effect of Partial Pressure of N_2 on Nitrogen Fixation Rate

To verify the effect of N_2 partial pressure on the nitrogen fixation rate, we performed two control experiments with different gas feeding at 400 ℃ for 4 hours in the molten hybrid system (Figure 3a**)**. In the first experiment, N_2 (5 cm^3/min) and Ar (15 cm^3/min) were fed to the liquid alloy and molten salt, respectively. In the second experiment, the mixture of N_2 (5 cm^3/min) and Ar (15 cm^3/min) were fed to the liquid alloy. The Li in the alloy reacted with N_2 to form Li_3N that floated up and was dissolved in the molten LiCl-KCl above. After cooling, five pieces of solidified salt samples were collected from each experiment to determine the nitrogen fixation rate according to Eq. S1. In the case of feeding the mixture of N_2 and Ar, the N_2 partial pressure was only 0.25 atm, and the nitrogen fixation rate was as low as 41.6 μg/s. In comparison, when feeding the N_2 and Ar to the liquid alloy and the molten salt, respectively, the nitrogen fixation rate was larger (53.5 μg/s). The results verified that the rate of nitrogen fixation by the liquid alloy increased with the N_2 partial pressure.

Table S5. Activity levels of molten catalytic systems studied in this work and several relevant catalytic materials that operated at 1 bar as reported in literature. The activity level in this work is calculated by dividing the amount of ammonia product by the reaction time and the total mass of the alloy and the salt. The materials labelled with * were tested with the stepwise chemical looping route in which N_2 and H_2 were fed separately to the system. All the other materials were tested with catalytic processes of flowing N_2 and H_2 at the same time into the reactors.

Materials	T (°C)	P (bar)	Average amount of NH_3 produced per hour (μmol h^{-1})	Total mass of catalyst (g_{cat})	Activity level (μmol g_{cat}^{-1} h^{-1})	Refer-ences
70mol%Li-Zn (5cm) and LiCl-KCl (5cm)	400	1	2.605	21.55	0.121	This work
70mol%Li-Zn (5cm) and LiCl-KCl (10cm)	400	1	4	30.35	0.132	
70mol%Li-Zn (5cm) and LiCl-KCl (15cm)	400	1	5.361	39.15	0.137	
Pure Na	500	1	1.501	20	0.075	5
LiH *	350	1	1.44	0.03	48	6
Zn-8LiH *	350	1	28.68	0.03	956	
50wt%Ni-LiH	350	1	undetectable	0.03	undetectable	7
50wt%Ni-LiH *	300	1	45.99	0.03	1533	
LaMnSi	400	1	12	0.1	120	8
LaFeSi	400	1	62	0.1	620	
LaCoSi	400	1	122.5	0.1	1225	
Cs-promoted Ru/MgO	350	1	300	0.03	10000	9

Note S7. Computational details

All the *ab initio* molecular dynamics (AIMD) simulations and density functional theory (DFT) calculations were performed with Vienna Ab initio Simulation Package (VASP).[10, 11] The generalized gradient approximation (GGA) combined with the Perdew−Burke−Ernzerhof (PBE) functional was utilized to depict the core-electron interactions. The Grimme DFT-D3 correction method was employed to take the van der Waals interaction term into account. The energy convergence threshold is 10^{-4} eV. Considering the large supercell, Γ-point of Brillouin zone and 350 eV cut-off energy were used in the AIMD calculations.

The AIMD calculations were performed with NVT ensemble, in which the temperature was kept by Nose-Hoover thermostat. The time step was set as 1 fs. To calculate the free-energy change during a reaction, we utilized the slow-growth method implemented in VASP. In such calculations, a collective variable (CV, ξ) was assigned to describe the geometric property along the reaction path. Here the N–N bond distance $d_{\text{N-N}}$ was chosen as the CV, serving as the reaction coordinate. Free energy samplings were performed with constrained $d_{\text{N-N}}$ in the simulations. Consider states *a* and *b* during a reaction, the work needed for the transformation from state *a* to state *b* can be calculated through integrating the potential energies V through CV using the following formula:

$$\Delta W_{a\to b} = \int_{\xi(a)}^{\xi(\mathrm{b})} \left(\frac{\partial V}{\partial \xi}\right)_{\xi} \mathrm{d}\xi.$$

The obtained works $\Delta W_{a\to b}$ could be related to the free energy change $\Delta A_{a\to b}$ via Jarzynski equality theorem[12]:

$$\mathrm{e}^{-\Delta A_{a\to b}/k_B T} = \overline{\mathrm{e}^{-\Delta W_{a\to b}/k_B T}}$$

where k_{B} is the Boltzmann constant, and the expression of $\bar{x}$ denotes a canonical averaging over *x*. For each reaction, we computed 3 trajectories to obtain *W* along the reaction path. The corresponding increment speed of CV was 10^{-4} Å/step. The total simulation step is 30000, and the overall simulation time is 30 ps. The initial structures of the slow-growth calculations were obtained by performing at least 5 ps equilibrium

MD simulations to allow the liquid catalyst around the N_2 molecule to find the favorable arrangements, with the $d_{N\text{-}N}$ constrained to be 1.0 Å, slightly smaller than the equilibrium $d_{N\text{-}N}$ of 1.3 Å in the Li-Zn alloy. As the simulation progressed, the $d_{N\text{-}N}$ gradually increased from 1.0 Å to 4.0 Å, which covered the range of the N_2 cleavage process and allowed for the derivation of the free energy profile changes along $d_{N\text{-}N}$. The initial, transition, and final states were determined from the local minimum or maximum points in the free energy profiles, respectively.

The coordination number (CN) of an atom *i* were defined by:

$$CN = \sum_j \frac{1 - \left(r_{ij}/r_0\right)^{nn}}{1 - \left(r_{ij}/r_0\right)^{nd}}$$

where r_{ij} was the distance between atoms *i* and *j*, *nn*, *nd* and r_0 were set to 9, 14 and 1.2 Å respectively.

References for the Electronic Supplementary Information

1. H. Okamoto, *J. Phase Equilibria Diffus.*, 2012, **33**, 345-345.
2. S. Hino, N. Ogita, M. Udagawa, T. Ichikawa and Y. Kojima, *J. Appl. Phys.*, 2009, **105**, 023527.
3. H. Ning, Z. Lan, J. Bai and J. Guo, *Mater. Chem. Phys.*, 2014, **144**, 484-490.
4. W. Gao, J. Guo and P. Chen, *Chin. J. Chem* . 2019, **37**, 442-451.
5. F. Kawamura and T. Taniguchi, *Sci. Rep.*, 2017, **7**, 11578.
6. R. Wang, W. Gao, S. Feng, Y. Guan, Q. Wang, J. Guo and P. Chen, *ChemSusChem*, 2023, **16**, e202300813.
7. W. Gao, J. Guo, P. Wang, Q. Wang, F. Chang, Q. Pei, W. Zhang, L. Liu and P. Chen, *Nat. Energy*, 2018, **3**, 1067-1075.
8. H. Li, Y. Gong, H. Yang, X. Yang, K. Li, J. Wang and H. Hosono, *ChemSusChem*, 2023, **16**.
9. Q. Wang, J. Pan, J. Guo, H. A. Hansen, H. Xie, L. Jiang, L. Hua, H. Li, Y. Guan, P. Wang, W. Gao, L. Liu, H. Cao, Z. Xiong, T. Vegge and P. Chen, *Nat. Catal.*, 2021, **4**, 959-967.
10. G. Kresse and J. Hafner, *Phys. Rev. B*, 1993, **47**, 558-561.
11. G. Kresse and J. Furthmüller, *Comp. Mater. Sci.*, 1996, **6**, 15-50.
12. C. Jarzynski, *Phys. Rev. Lett.*, 1997, **78**, 2690-2693.